Thermal Contact Resistance: Effect of Elastic Deformation

M. Bahrami [1], and M. M. Yovanovich , and J. R. Culham
Microelectronics Heat Transfer Laboratory
Department of Mechanical Engineering, University of Waterloo
Waterloo, ON, Canada
[1] Corresponding author, e-mail: majid@mhtlab.uwaterloo.ca

Abstract

Existing models over-predict the thermal contact resistance of conforming rough joints at low contact pressures. However, the applicable pressure range in the microelectronics industry is low due to load constraints. In this paper a new model is presented which is more suitable for low pressures. The present model assumes plastic deformation at microcontacts. The effect of elastic deformations beneath the microcontacts is determined by superimposing normal deformations in an elastic half-space due to adjacent microcontacts. The model also accounts for the variation of the effective microhardness. A parametric study is conducted to investigate the effects of main contact input parameters on the elastic effect. The study reveals that the elastic deformation effect is an important phenomenon especially in low contact pressures. The present model is compared with experimental data and good agreement is observed at low contact pressures.

Keywords

Thermal Contact Resistance, Plastic Deformation, Elastic Deformation, Low Contact Pressure, Microhardness, Half-space, Roughness, Modeling, Experimental Data.

Nomenclature

A = area, m2
a = radius of microcontacts, *m*
b_L = specimen radius, m
c_1, c_2 = Vickers microhardness coefficients
E = Young's modulus, *Pa*
E' = effective elastic modulus, *Pa*
F = applied load, N
H_{mic} = microhardness, Pa
H^* = non-dimensional microhardness H_{mic} / E'
k = thermal conductivity, *W/mK*
L = distance between microcontacts, *m*
m = combined mean absolute surface slope
n = number of microcontacts
P = apparent contact pressure, *Pa*
R_j = thermal joint resistance, *K/W*
r = radial position, *m*
x = non-dimensional position, *r/L*
Y = mean surface plane separation, *m*

Greek

γ = plasticity index, $H_{mic} / E' m$
ε = relative radius, $\sqrt{A_r / A_a}$
η = density of microcontacts, m^{-2}
Λ = non-dimensional length, $b_L^2 / (\sigma / m)$
λ = non-dimensional separation, $Y / \sqrt{2}\sigma$
σ = combined RMS surface roughness, *m*
υ = Poisson's ratio
ω = normal elastic deformation, *m*

Subscripts

0 = pure plastic model value
1,2 = solid *1, 2*
a = apparent
r = real
s = solid, micro

1. Introduction

The continued growth in performance and functionality of microelectronic and avionic systems has resulted in a significant increase in heat dissipation rates and presents a great challenge to thermal engineers. The heat generated must pass through a complex network of thermal resistances to dissipate from the junction to the surroundings. A significant resistance in the network is the thermal constriction/spreading resistance through microcontacts at the interface between the package and its heat sink. Therefore, an accurate knowledge of mechanics of the contact, i.e. number and size of microcontacts, is essential for the thermal resistance analysis.

When random rough surfaces are placed in mechanical contact, *real contact* occurs at the summit of surface asperities which are called microcontacts. The real contact area, A_r, the summation of the microcontacts, forms a small portion of the nominal contact area, typically a few percent of the nominal contact area. The contact between two Gaussian rough surfaces is modeled by the contact between a single Gaussian surface, that has the combined characteristics of the two surfaces, with a perfectly smooth surface. The combined roughness, σ, and surface slope, *m*, can be found from

$$\sigma = \sqrt{\sigma_1^2 + \sigma_2^2} \quad m = \sqrt{m_1^2 + m_2^2} \tag{1}$$

To study the constriction/spreading resistance of microcontacts, the joint is usually studied in a vacuum where the heat transfer between contacting bodies occurs only via conduction through microcontacts. Thermal Contact Resistance (TCR) of conforming rough surfaces in a vacuum is proportional to the real contact area [1]. TCR can be decreased by reducing the roughness and out-of-flatness of the surfaces before the interface is formed or increasing contact

pressure. However, manufacturing highly finished surfaces is not practical due to cost constraints. Also, load constraints on electronic components make it unfeasible to use high contact pressure.

Very little has been done for light pressures <0.1 MPa, which is the applicable range for microelectronics devices. Existing models such as [2,3] can predict TCR for moderate to high contact pressures accurately. Milanez et al. [4] experimentally studied low contact pressure joints in a vacuum and showed that the models [2,3] overestimate the TCR at low pressures. They called this phenomenon the *truncation effect* and attributed this trend to the Gaussian assumption of the surface asperities which implies that asperities with *infinite* heights exist. Milanez et al. [4] proposed correlations for maximum asperities heights as functions of surface roughness.

Existing plastic models [2,3] do not consider the effect of elastic deformations beneath the microcontacts. These effects would be negligible if the elastic modulus of contacting bodies were infinity and/or the distance between the neighboring microcontacts was small enough so the elastic deformation was the same for all microcontacts. In reality, none of the above is true and the elastic deflection underneath a microcontact is always larger than the deformation outside the microcontact area (mean plane). Mikic [5] was the first one to point out this problem and proposed a model. However, his model did not consider the effect of the elastic deformation of neighboring microcontacts and variation in the effective microhardness which was reported later by Hegazy [6]. Also Mikic did not compare his model against experimental data.

2. Problem Statement

Figure 1 shows the cross-section of the contact schematically; note that the surface slopes of asperities, *m*, is exaggerated. In reality, the surface asperities can be visualized as shallow hills and valleys. In this study the microcontacts are assumed to deform plastically, reasons supporting this assumption are discussed in the next section.

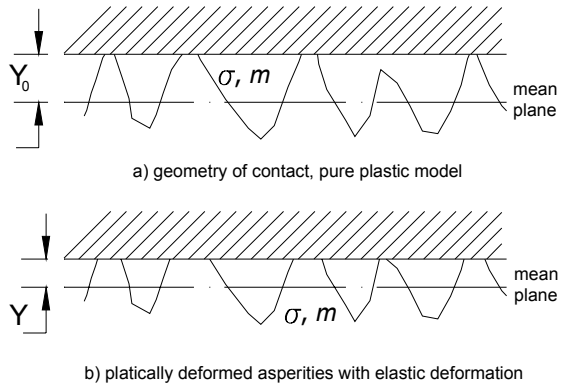

Fig.1. Effect of elastic deformation on mean separation

Consider plastically deformed microcontacts as loaded areas on an elastic half-space. The pressure applied on the microcontacts is the effective microhardness of the joint. As elastic deformations occur beneath the plastic microcontacts, mean separation between the two contacting surfaces decreases, compared with the value predicted by the pure plastic model where the elastic deformation is neglected, i.e. $Y<Y_0$. As a result of smaller separation, more microcontacts are formed which in turn leads to a higher real contact area that is equivalent to a lower TCR.

The goal of this study is to investigate the effect of elastic deformations beneath the plastically deformed microcontacts on TCR. A new model is proposed that accounts for the elastic deformation of microcontacts and variation of effective microhardness with mean radius of microcontacts. A novel numerical algorithm is presented that satisfies the force balance. The present model is compared with experimental data.

3. Why Plastic Microcontacts?

Different approaches have been taken to analyze the deformation of asperities by assuming plastic [2], elastic [7], or elastoplastic [8,9] regimes at microcontacts. It has been observed through experiments that the real contact area is proportional to the applied load [10]. However, if simple elastic deformation, following the Hertzian theory, is assumed for asperities, the real contact area will not be linearly proportional to the load, instead one obtains, $A_r \propto F^{2/3}$. Greenwood and Williamson (GW) [7] developed an elastic contact model. They proposed that as the load increases new microcontacts are nucleated while the mean size of microcontacts remains constant; the GW model satisfied the observed proportionality, $A_r \propto F$. As a result, an *effective elastic microhardness* can be defined for elastic models which shows that the assumption of elastic and/or plastic deformation of asperities leads to similar results [7,11]. Greenwood and Williamson [7] introduced a plasticity index as a criterion for plastic flow of microcontacts. They reported that the load has little effect on the deformation regime. Based on plasticity index, Greenwood and Williamson concluded that except for especially smooth surfaces, the asperities will flow plastically under the lightest loads. Considering an indentation hardness for asperities, Persson [12] also concluded that except for polished surfaces all microcontacts deform plastically. Mikic [5] proposed a plasticity index, $\gamma=H_{mic}/E'm$, to determine the deformation mode of asperities

$$\begin{cases} \gamma \le 0.33 & \text{asperities deform plastically} \\ \gamma > 3.00 & \text{asperities deform elastically} \end{cases} \tag{2}$$

the effective elastic modulus is defined as

$$\frac{1}{E'} = \frac{1-\upsilon_1^2}{E_1} + \frac{1-\upsilon_2^2}{E_2}$$

Mikic [5] also concluded that for most engineering surfaces the asperity deformation mode is plastic and the average asperity pressure is the joint effective microhardness. According to [5], the deformation mode of asperities depends on material properties and the shape of asperities; also it is not a function of the applied load.

4. Microhardness

Microhardness can vary throughout the material as the indentation depth is increased [13]. Microhardness depends on several parameters, mean surface roughness, mean slope of asperities, method of surface preparation, and applied pressure. Depending on the surface preparation, microhardness can be much greater than the bulk hardness [6,12]. As shown in Fig. 2, microhardness decreases with increasing depth of the indenter until bulk hardness is obtained. Hegazy [6] concluded that this increase in the plastic yield stress (microhardness) of the metals near the free surface is a result of local extreme work hardening or some surface strengthening mechanism. He proposed empirical correlations to account for the decrease in microhardness with increasing depth of penetration

$$H_{mic} = c_1 \left(d_v / d_0 \right)^{c_2} \quad \text{and} \quad d_0 = 1 \mu m \tag{3}$$

where $d_v = 7t$ is the Vickers indentation diagonal in micrometers. The correlation coefficients c_1 and c_2 are determined from Vickers microhardness measurements. Equation (3) is general and can also be used for surfaces that have a constant microhardness, $H_{mic,e}$, by substituting $c_1 = H_{mic,e}$ and $c_2 = 0$.

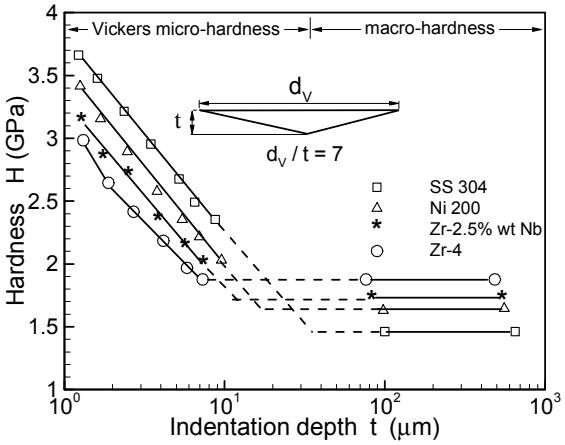

Fig. 2. Measured hardness and microhardness [6]

Song and Yovanovich [14] proposed a correlation to calculate microhardness as follows:

$$\frac{P}{H_{mic}} = \left[\frac{P}{c_1 \left(1.62 \sigma' / m \right)^{c_2}} \right]^{\frac{1}{1+0.071 c_2}} \tag{4}$$

5. Pure Plastic Models

Cooper et al. (CMY) [2], based on the level-crossing theory and using the sum surface approximation, derived relationships for mean microcontact size, a, and density of microcontacts, η, by assuming hemispherical asperities whose heights and slopes have Gaussian distributions

$$a = \sqrt{\frac{8}{\pi}} \left(\frac{\sigma}{m} \right) \exp\left(\lambda^2 \right) \operatorname{erfc}(\lambda)$$
$$\eta = \frac{1}{16} \left(\frac{m}{\sigma} \right)^2 \frac{\exp\left(-2\lambda^2 \right)}{\operatorname{erfc}(\lambda)} \tag{5}$$

where λ is the dimensionless separation. They also showed that the ratio of the real contact area to the apparent area is related to the mean separation

$$\frac{A_r}{A_a} = \frac{P}{H_{mic}} = \frac{1}{2} \operatorname{erfc}(\lambda) \tag{6}$$

where H_{mic} is the effective microhardness of the softer material in contact and, $P = F/A_a$, is the nominal contact pressure.

Pullen and Williamson [15] experimentally investigated plastic flow under large loads. They assumed that material displaced from the contacting regions must reappear by raising some parts of the non-contacting surface. They assumed that the volume of material remained constant and that the material that is plastically displaced appears as a uniform rise over the entire surface. Since the uniform rise will not affect the shape of the surface outside the contact area, they showed that the contact area due to the interaction of microcontacts is not proportional to the normal load at relatively high loads; and proposed as a good approximation; $A_r / A_a = P_p / \left(1 + P_p \right)$, where $P_p = P_m / H_{mic}$.

6. Present Model

The modeled geometry of the contact is shown in Fig. 3. Nine microcontacts, named *A* to *I,* are shown in Fig. 3 as hatched identical circles of radius, *a*. The microcontacts are assumed to be arranged in a square array where the shortest distance between neighboring microcontacts is *L*. From Fig. 3, one can calculate the relative radius as

$$\varepsilon = \sqrt{\frac{A_r}{A_a}} = \sqrt{\pi} \frac{a}{L} \tag{7}$$

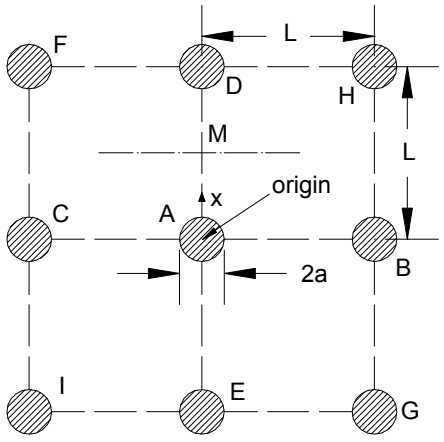

Fig. 3. Modeled geometry of contact plane.

The normal elastic displacement of a half-space produced as a result of applying a uniform pressure distribution H_{mic} over a circular area of radius a can be determined from [16]

$$\omega = \begin{cases} \dfrac{4H_{mic}a}{\pi E'} E\left(\dfrac{r}{a}\right) & r \le a \\ \dfrac{4H_{mic}r}{\pi E'}\left[E\left(\dfrac{a}{r}\right) - \left(1-\dfrac{a^2}{r^2}\right)K\left(\dfrac{a}{r}\right)\right] & r \ge a \end{cases} \quad (8)$$

where r is the radial location measured from the center of the loaded area; and E(.) and K(.) are the complete elliptic integrals of the second and the first kind, respectively. The mean elastic deformation of the loaded circular area is: $\varpi = 16H_{mic}a/3\pi E'$.

Equation (8) can be non-dimensionalized and re-arranged in the following form:

$$\omega = \begin{cases} \dfrac{\varepsilon}{\sqrt{\pi}} E\left(\dfrac{\sqrt{\pi}x}{\varepsilon}\right) & x \le \dfrac{\varepsilon}{\sqrt{\pi}} \\ x\left[E\left(\dfrac{\varepsilon}{\sqrt{\pi}x}\right) - \left(1-\dfrac{\varepsilon^2}{\pi x^2}\right)K\left(\dfrac{\varepsilon}{\sqrt{\pi}x}\right)\right] & x \ge \dfrac{\varepsilon}{\sqrt{\pi}} \end{cases} \quad (9)$$

where

$$\omega = \frac{4H_{mic}L}{\pi E'}\omega^* = \frac{4H_{mic}a}{\pi E'\varepsilon}\omega^* \quad (10)$$

and $x=r/L$. Relationship for the deformation outside the contact area, i.e., $x \ge \varepsilon/\sqrt{\pi}$ is complex as given in Eq. (9). The following simpler relationship can be used to calculate the deformation of a half-space outside the loaded area over a wide range of x and ε with a reasonable accuracy:

$$\omega^* = \frac{0.26\varepsilon^2}{x} \qquad x > \frac{\varepsilon}{\sqrt{\pi}} \quad (11)$$

The elastic deformation of a half-space is linear, thus superposition can be applied to calculate the total elastic deformation due to the microcontact "*A*" and neighboring microcontacts.

The line AM, Fig. 3, is chosen as a representative (or mean plane) of the half-space to estimate the total elastic deformations due to microcontacts A to I. Using superposition the elastic deformation of the mean plane AM is

$$\omega_{AM} = \omega_A + \omega_D + \omega_E + 2\omega_B + 2\omega_H + 2\omega_G \quad (12)$$

where due to symmetry $\omega_B = \omega_C$, $\omega_G = \omega_I$, and $\omega_F = \omega_H$.

The non-dimensional mean elastic deformation underneath the microcontact *A*, $0 < x < \varepsilon/\sqrt{\pi}$, due to its neighbors and itself is

$$\overline{\omega_1^*} = \frac{4\varepsilon}{3\sqrt{\pi}} + 0.52\pi\int_0^{\frac{\varepsilon}{\sqrt{\pi}}} \sum \frac{x}{a_i x + b_i} dx \qquad x < \frac{\varepsilon}{\sqrt{\pi}} \quad (13)$$

where a_i and b_i are the constants due to changing the location of the origin from each neighboring microcontact to the center of the microcontact "*A*". Using the same method, the mean deformation for the rest of the mean plane *AM*, i.e., $\varepsilon/\sqrt{\pi} \le x \le 1/2$ can be found:

$$\overline{\omega_2^*} = \frac{0.52\varepsilon^2}{0.25 - \varepsilon^2/\pi}\int_{\frac{\varepsilon}{\sqrt{\pi}}}^{1/2} \sum \frac{x}{a_i x + b_i} dx \qquad \frac{\varepsilon}{\sqrt{\pi}} \le x \le \frac{1}{2} \quad (14)$$

Finally the mean elastic deformation of the mean plane *AM* can be calculated using $\overline{\omega_1^*}$ and $\overline{\omega_2^*}$.

Figure 4 shows the mean deformation due to microcontact A only, total mean deformation considering the effects of neighbors, and the net elastic displacement for the microcontact "*A*" as the relative radius of microcontacts ε varies. As expected, for small values of ε i.e. *<0.01* relatively low contact pressure, the effects of neighboring microcontacts is small and can be ignored. As ε increases, the effect of neighboring microcontacts become more significant, also the displacement of the mean plane increases. As a result of these two competing trends, the net elastic deformation beneath the microcontact "*A*" becomes smaller and eventually the net displacement approaches zero at relatively large loads.

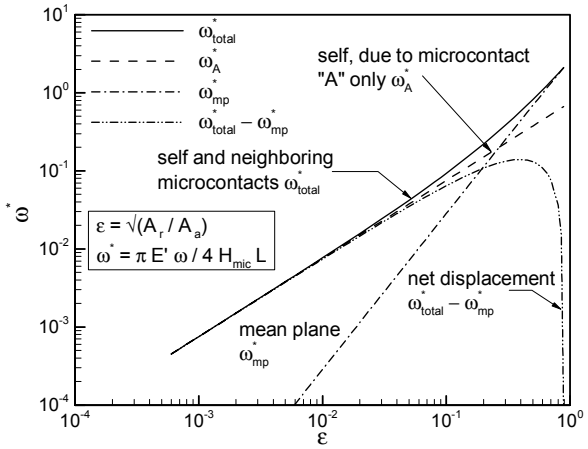

Fig. 4. Elastic deformation beneath microcontact *A*, for $0 < x < \varepsilon/\sqrt{\pi}$

6.1. Numerical Algorithm

A new numerical model is developed to account for the elastic deformation beneath microcontacts and variations in microhardness. The numerical algorithm used in the present model is described below and is shown in Fig. 5.

Cooper et al.'s (CMY) [2] relationships, Eqs. (5), (6) are used to calculate the mean radius a_0, density η_0, relative radius ε_0, and mean separation of the joint λ_0. Song and Yovanovich correlation [14], Eq. (4), is employed to estimate an effective microhardness H' for the pure plastic model. The subscript "*0*" indicates the pure plastic model values.

The net mean elastic deformation, $\omega_{net} = \omega_1 - \omega_{AM}$, is then calculated using relative radius ω_0 as described in the previous section. A new mean separation between contacting surfaces can be found from

$$\lambda = \lambda_0 - \omega_{net}/\sqrt{2}\sigma \quad (15)$$

With new separation λ, one can determine a new density of microcontacts η from Eq. (5). Applying a force balance, a new mean radius of microcontacts a is determined from

$$a = \sqrt{\frac{F}{\pi H_{mic} A_a \eta}} \tag{16}$$

Since the mean radius of the microcontacts changes as the applied load varies, the microhardness will also change according to Eq. (3). If the print area in a Vickers test is assumed to be equal to the microcontact area, a relation between the Vicker's diagonal and the mean size of microcontacts can be found as

$$d_v = \sqrt{2\pi}a \tag{17}$$

Therefore, a new effective microhardness can be computed from the new radius of microcontacts. This procedure continues until the difference between the new mean radius of microcontacts a and the old one a_0 becomes negligible. The results of the above procedure, i.e. the mean radius and the density of microcontacts, are used to calculate the TCR of the joint. The thermal resistance analysis is based on the premise that there are n ($=\eta A_a$) identical circular microcontacts of radius a that provide n parallel paths for thermal energy to be transferred in the contact plane. The constriction/spreading resistance of the joint then can be determined by employing the flux tube solution [13] as:

$$R_j = \frac{(1-\varepsilon)^{1.5}}{2k_s a \eta A_a} \tag{18}$$

where $k_s=2k_1k_2/(k_1+k_2)$ is the harmonic mean of thermal conductivities of the contacting bodies.

6.2. Trends of Contact Parameters

The present model is run for a joint as the applied load is varied over a wide range to study the trends of the contact parameters; see Figs. 6 and 7 for the contact input parameters. The contact parameters calculated by both the present and the pure plastic models are listed in Table 1.

F (N)	pure plastic model				present model			
	λ_0	ε_0	a_0 (μm)	η_0	λ	ε	a (μm)	η
0.001	4.88	1.57E-6	4.76	0.03	4.77	2.66E-6	4.71	0.10
0.01	4.63	5.47 E-6	5.01	0.38	4.52	8.38E-6	4.65	1.03
0.1	4.36	1.89 E-5	5.31	4.03	4.25	2.65E-5	4.66	10.31
1	4.07	6.45 E-5	5.66	41.34	3.96	8.41E-5	4.74	100.1
5	3.87	1.51 E-4	5.94	205.94	3.75	1.89E-4	4.86	481.1
10	3.77	2.18 E-4	6.08	408.69	3.66	2.68E-4	4.93	940.7
50	3.55	5.07 E-4	6.44	1975.3	3.43	6.03E-4	5.13	4396.6
100	3.45	7.28 E-4	6.61	3864.6	3.33	8.57E-4	5.25	8481.1
200	3.35	1.05 E-3	6.80	7524.41	3.23	1.22E-3	5.38	16282
1000	3.10	2.41 E-3	7.30	34627.8	2.97	2.76E-3	5.78	72497
2000	2.99	3.44 E-3	7.55	66171	2.86	3.93E-3	6.00	136509
5000	2.84	5.51 E-3	7.91	154167	2.70	6.27E-3	6.34	311572
10000	2.71	7.85 E-3	8.23	289821	2.58	8.95E-3	6.65	575983
20000	2.59	1.12 E-2	8.58	540371	2.45	1.28E-2	7.03	1054370
50000	2.42	1.78 E-2	9.13	1213824	2.27	2.05E-2	7.63	2303327

Table 1. Contact parameters calculated by present and pure plastic models.

Figures 6 and 7 show the ratio of the contact parameters as the non-dimensional pressure P/H_{mic} is increased. As shown in these plots, the ratio of separations λ/λ_0 is greater than one for the entire comparison due to elastic deformations effect. As a result of smaller separation, more microcontacts are formed i.e. $n/n_0>1$, the real contact area is increased A_r/A_{r0}, thus thermal resistance is decreased $R_{j0}/R_j>1$. It can also be seen that these ratios A_r/A_{r0}, n/n_0, and R_{j0}/R_j decrease as the applied load increases which indicates that the elastic deformation effect becomes less important at higher loads. This is consistent with the trend seen in Fig. 4.

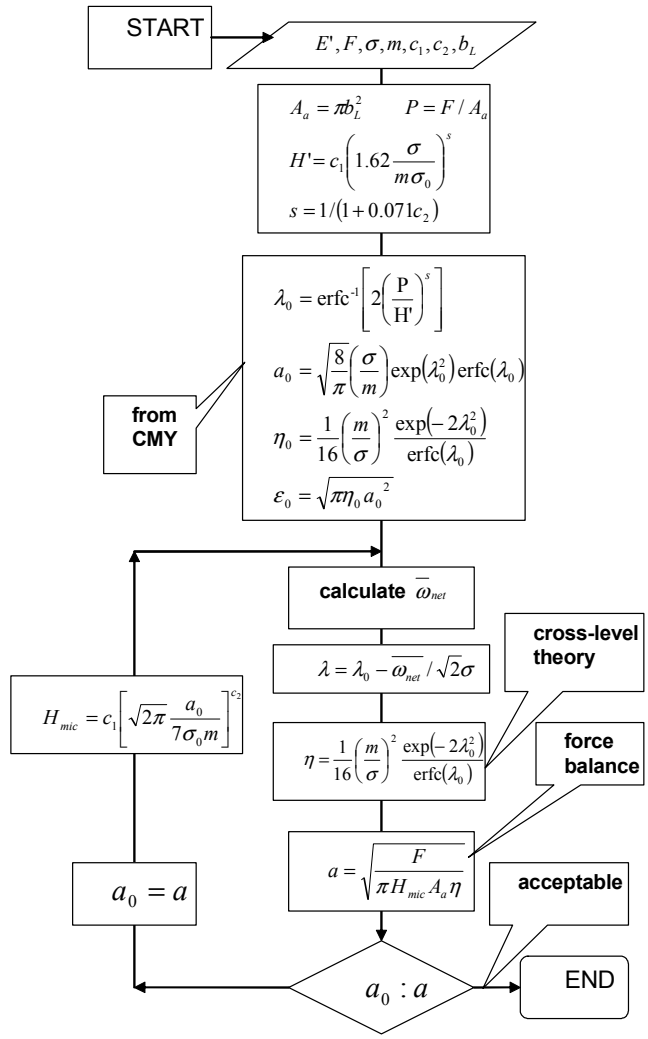

Fig. 5. Numerical algorithm used in present model.

Figure 6 shows that the ratio of microcontacts radius $a/a_0<1$ throughout the comparison. However, it should be noted that the absolute radius of microcontacts, a, increases by increasing the load, see Table 1. Therefore, the effective microhardness H_{mic} decreases as the load increases, see Eqs. (17) and (3). The effective microhardness shown in Fig. 6 is non-dimensionalized with respect to $H'=c_1(1.62/m)^{c2}$. Note that, H', remains constant throughout the comparison.

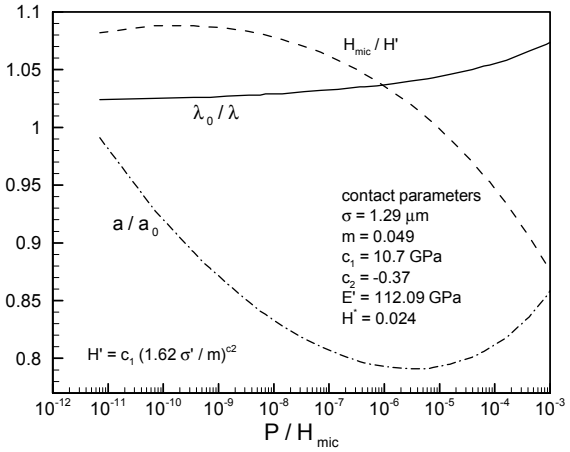

Fig. 6. Ratio of calculated values by present model over pure plastic model for: mean separation, mean radius of microcontacts, and effective microhardness.

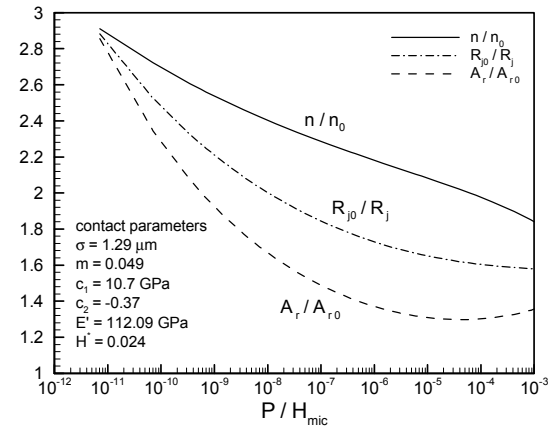

Fig. 7. Ratio of calculated values by present model over pure plastic model for: density of microcontacts, real contact area, and TCR.

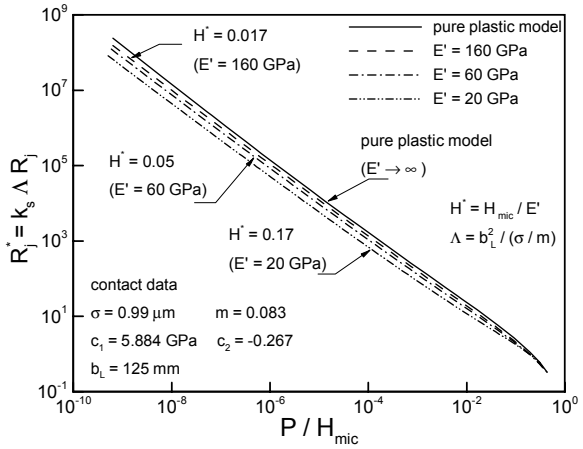

Fig. 8. Effect of elastic modulus on present model.

6.3. Effect of Elastic modulus

Non-dimensional joint resistances of a typical joint is shown in Fig. 8 over a wide range of the non-dimensional pressure P/Hmic. Four values of $E^{'}$=20, 60, 160, and infinity (pure plastic model) have been selected to investigate the effect of elastic modulus on TCR. The contact input parameters are shown in the figure and are kept constant as the effective elastic modulus is changed. The ratio of the effective microhardness over the effective elastic modulus $H^{*}=H_{mic}/E^{'}$ is used as to label these four curves. It can be seen that as H^{*} approaches zero, i.e. $E^{'}\rightarrow infinity$ the present model approaches the pure plastic model and the elastic effect vanishes. Therefore, it may be concluded that the non-dimensional parameter, H^{*}, is a measure of how significant is the elastic deformation effect. Also note that the difference between the present model and the pure elastic model decreases as P/H_{mic} increases. Beyond a certain pressure the difference between the pure plastic model and the present model (three values of $E^{'}$) becomes negligible. This is in agreement with the observed trend in Fig. 4 which indicates that the effect of elastic deformation is more important at lighter loads.

6.4. Effect of Roughness

To study the effect of roughness on the elastic deformation effect, the present model is run over a range of applied load for a typical contact. Four levels of roughness, i.e. 0.5, 1, 2, and 5 μm are chosen. The predicted joint resistances by the present model are normalized with respect to the pure plastic model resistances R_{j0}/R_j and plotted versus the non-dimensional pressure P/H_{mic} in Fig. 9. The contact input parameters are shown in the figure and are kept constant as roughness level is changed. The effective microhardness is assumed to be a constant, i.e. it is not a function of the penetration depth or microcontacts radius by setting $c_2=0$, to investigate the effect of roughness only.

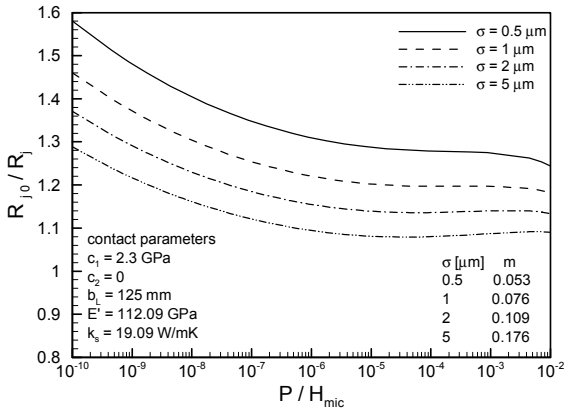

Fig. 9. Effect of surface roughness on present model.

As shown in Fig. 9, at a fixed non-dimensional pressure P/H_{mic}, the elastic effect is larger at smaller roughness levels. This phenomenon can be explained as follows. The averaged non-dimensional net elastic deformation beneath

microcontacts $\overline{\omega^*_{net}}$ is a function of relative radius, ε, only which is a function of the non-dimensional pressure P/H_{mic}, see Eq. (6). Therefore, at a fixed ε or P/H_{mic} the net deformation $\overline{\omega^*_{net}}$ is the same for all roughness levels. However, from Eqs. (10) and (15), one can conclude that the reduction in the mean separation λ, due to the elastic effect, is proportional to the ratio of a/σ, where relative radius ε and microhardness P/H_{mic} are constant. For smaller roughness levels, the ratio a/σ is larger; therefore the net reduction in the non-dimensional separation λ is larger. This leads to more new microcontacts, larger real contact area and therefore less TCR or equivalently more elastic effect.

7. Comparison with Data

The present model is compared with experimental data of Milanez et al. [4] in Figs. 10 to 12. They collected three sets of data for SS 304, the surface parameters of each test are listed in the corresponding plot. The pure plastic model is included in the comparisons to better show the effect of elastic deformation. The average difference between the present model and the pure plastic model over the applied load range is also reported in the comparisons. The non-dimensional parameter H^* is also shown for each set of data where H_{mic} is an average value of the effective microhardness over the comparison range. As shown in the plots, the data of [4] show a better agreement with the present model at relatively low loads and move toward the pure plastic model at higher loads.

The three sets of [4] data differ only in roughness levels which are 0.72, 1.29, and 3.07 μm. From Figs. 10 to 12 can be seen that the difference between the present model and the pure plastic model becomes smaller at data set T3 where surface roughness is the largest of the three sets of data. This is consistent with the trend seen in Fig. 9.

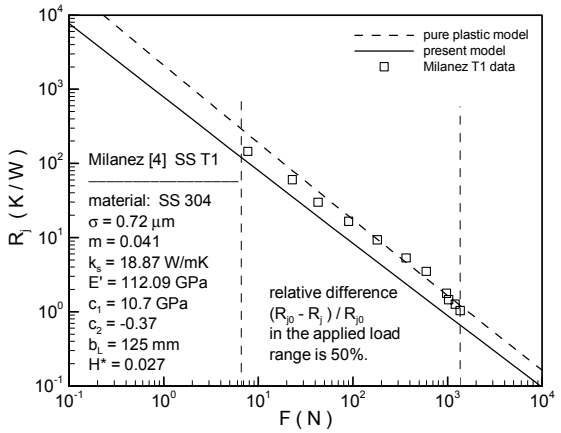

Fig. 10. Comparison of present model with Milanez et al. [4] data, test T1.

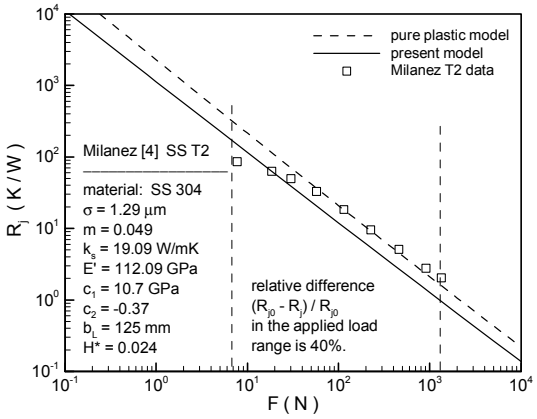

Fig. 11. Comparison of present model with Milanez et al. [4] data, test T2.

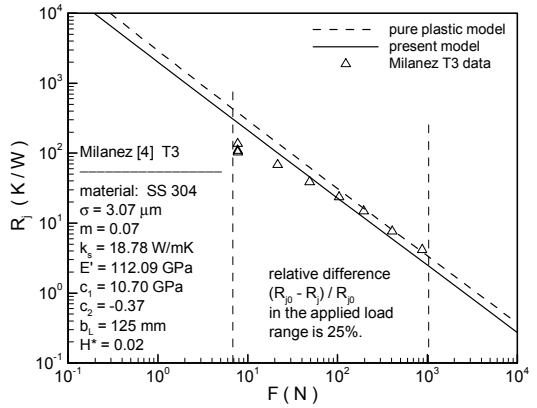

Fig. 12. Comparison of present model with Milanez et al. [4] data, test T3.

The present model is also compared with experimental data of Hegazy [6] in Figs. 13 to 15. Hegazy conducted several experiments with four different alloys. Here, three different materials are chosen, i.e. Zr-2.5%wt. Zircaloy 4 and nickel 200; which cover a relatively wide range of contact input parameters elastic modulus, roughness, thermal conductivity, and microhardness coefficients. The material properties and surface parameters are listed in the figures. The data of [6] are closer to the present model at smaller loads and move toward the pure plastic model at larger loads, i.e. the same as Milanez et al. [4] data.

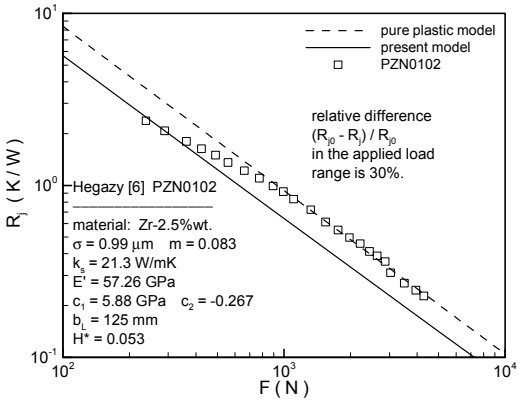

Fig. 13. Comparison of present model with Hegazy [6] data, test PZN0102.

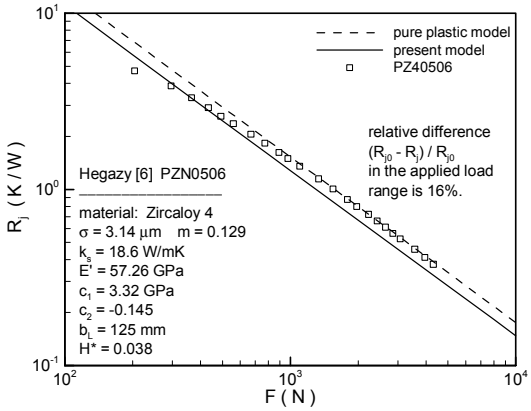

Fig. 14. Comparison of present model with Hegazy [6] data, test PZ40506.

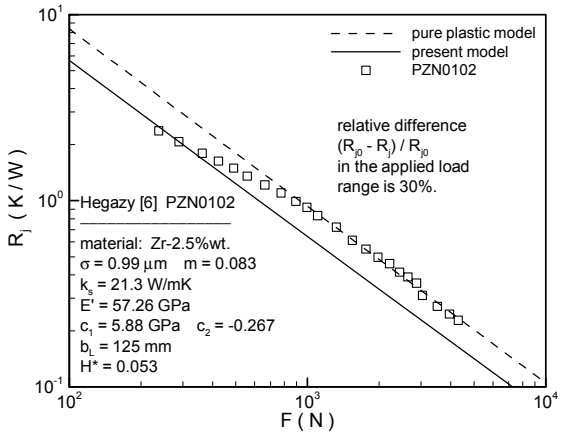

Fig. 15. Comparison of present model with Hegazy [6] data, test PNI0102.

Conclusions

The effect of elastic deformation of the substrate underneath the microcontacts is studied on the TCR of rough conforming joints in a vacuum. The microcontacts are assumed to deform plastically. A new model is developed that accounts for elastic deformations of the substrates due to self and neighboring microcontacts using superposition of elastic deformations in a half-space. The present model also accounts for the variation in the effective microhardness and satisfies the force balance.

The microcontacts are assumed as identical circles which are arranged in a square array. Relationships are derived for the average normal elastic deformation of the elastic substrate beneath microcontacts. The net elastic deformation of the microcontacts is calculated. Using the level-crossing theory, the mean separation between two contacting bodies is modified for the net elastic deformation. An iterative numerical algorithm is developed to compute the modified mean size, density, and the contact resistance of the joint. The force balance principle is used in the numerical solution.

The trends of the present model are studied and compared with the pure plastic model where the elastic deformation is completely ignored. It is observed that as a result of the elastic deformation the mean separations between two contacting surfaces becomes smaller; thus

- more microcontacts are nucleated,
- the real contact area is increased, and
- thermal contact resistance is decreased .

It is also shown that the elastic deformation effect becomes less important at higher loads. This is a direct result of that the net elastic deformation approaches zero at relatively high loads, i.e. the elastic deformation is uniform for the whole mean plane.

A parametric study is performed to investigate the effects of main input contact parameters on the joint resistance. A non-dimensional parameter $H^*=H_{mic}/ E'$ is introduced as a measure of importance of the elastic deformation. As H^* approaches zero, or $E' \rightarrow infinity$, the present model approaches the pure plastic model. It is also shown that for a fixed contact, the elastic effect is more significant at smaller roughness levels.

The present model is compared against experimental data of [4] and [6]. The experimental data cover a relatively wide range of input contact parameters. The data show good agreement with the present model at low contact loads. The data however move toward the pure plastic model at high contact loads. As a result of this trend, one can conclude that the present and the pure plastic models present lower and higher bounds for the thermal joint resistance of the conforming rough surfaces in a vacuum, respectively.

Acknowledgments

The authors gratefully acknowledge the financial support of the Centre for Microelectronics Assembly and Packaging, CMAP and the Natural Sciences and Engineering Research Council of Canada, (NSERC).

References

1. M. Bahrami, J.R. Culham, and M. M. Yovanovich, "Thermal contact resistance: A scale analysis approach," To be appeared in Journal of Heat Transfer, ASME, Also paper No. IMECE2003-44097, 2005.
2. M. G. Cooper, B. B. Mikic, and M. M. Yovanovich, "Thermal contact conductance," International

Journal of Heat and Mass Transfer, vol. 12, pp. 279-300, 1969.
3. M. M. Yovanovich, "Thermal contact correlations," AIAA Paper No. 81-1164, also Progress in Aeronautics and Aerodynamics: Spacecraft Radiative Transfer and Temperature Control, edited by T. E., Horton, vol. 83, pp. 83-95, 1982.
4. F. H. Milanez, M. M. Yovanovich, and, M. B. H. Mantelli, "Thermal contact conductance at low contact pressures," Journal of Thermophysics and Heat Transfer, vol. 18, pp. 37-44, 2003.
5. B. B. Mikic, "Thermal contact conductance; theoretical considerations," International Journal of Heat and Mass Transfer, vol. 17, pp. 205-214, 1974.
6. A. A. Hegazy, Thermal Joint Conductance of Conforming Rough Surfaces: Effect of Surface Micro-Hardness Variation, Ph.D. thesis, University of Waterloo, Dept. of Mech. Eng., Waterloo, Canada, 1985.
7. J. A. Greenwood and B. P. Williamson, "Contact of nominally flat surfaces," Proc., Roy. Soc., London, A295, pp. 300-319, 1966.
8. W. R. Chang, I. Etison, and D. B. Bogy, "An elastic-plastic model for the contact of rough surfaces," Journal of Tribology, vol. 109, pp. 257-253, 1987.
9. Y. Zhao, D. M. Maietta, and L. Chang, "An asperity model incorporating the transition from elastic deformation to fully plastic flow," Journal of Tribology, Trans. of ASME, vol. 122, pp. 86-93, 2000.
10. D. Tabor, The Hardness of Metals, Oxford University Press, Amen House, London E.C.4, UK, 1951.
11. J. A. Greenwood and J. H. Tripp, "The elastic contact of rough spheres," Transactions of the ASME: Journal of Applied Mechanics, vol. 89, no. 1, pp. 153-159, 1967.
12. N. J. Persson, Sliding Friction Physical Principles and Applications, Springer, Berlin, Germany, 2000.
13. M. M. Yovanovich and E. E. Marotta, Thermal Spreading and Contact Resistances, chapter 4, Heat Transfer Handbook, Editors: Bejan and D. Kraus, John Wiley and Sons Inc., Hoboken, New York, USA, 2003.
14. S. Song and M. M. Yovanovich, "Relative contact pressure: Dependence on surface roughness and Vickers microhardness," AIAA Journal of Thermophysics and Heat Transfer, vol. 2, no.1, pp. 43-47, 1988.
15. J. Pullen and B. P. Williamson, "On the plastic contact of rough surfaces," Proc., Roy. Soc., London, A327, pp. 159-173, 1972.
16. K. L. Johnson, Contact Mechanics, Cambridge University Press, Cambridge, UK., 1985.